Open access • Posted Content • DOI:10.21203/RS.3.RS-106760/V1

A COVID-19 antibody curbs SARS-CoV-2 nucleocapsid protein-induced complement hyper-activation — Source link

Sisi Kang, Mei Yang, Suhua He, Wang Yueming ...+16 more authors

Institutions: Sun Yat-sen University, Jinan University

Published on: 11 Sep 2020 - bioRxiv (Cold Spring Harbor Laboratory)

Topics: Epitope, Coronavirus, Monoclonal antibody, Antibody and Antigen

A COVID-19 antibody curbs SARS-CoV-2 nucleocapsid protein-induced complement hyperactivation

Sisi Kang
Sun Yat-sen University
Mei Yang
The Fifth Affiliated Hospital of Sun Yat-sen University
Suhua He
The Fifth Affiliated Hospital of Sun Yat-sen University
Yueming Wang
Jinan University; Zhuhai Trinomab Biotechnology Co., Ltd.
Xiaoxue Chen
Department of Experimental Medicine, Guangdong Provincial Key Laboratory of Biomedical Imaging, The Fifth affiliated Hospital, Sun Yat-sen University, Zhuhai, 519000
Yao-Qing chen
Sun Yat-sen University
Zhongsi Hong
Fifth Affiliated Hospital of Sun Yat-sen University
Jing Liu
The Fifth Affiliated Hospital of Sun Yat-sen University
Guanmin Jiang
Fifth Affiliated Hospital of Sun Yat-sen University
Qiuyue Chen
Sun Yat-sen University
Ziliang Zhou
Sun Yat-sen University https://orcid.org/0000-0002-6801-4180
Zhechong Zhou
Sun Yat-sen University
Zhaoxia Huang
Sun Yat-sen University
Xi Huang
Fifth Affiliated Hospital of Sun Yat-sen University
Huanhuan He
Guangdong Provincial Engineering Research Center of Molecular Imaging

Weihong Zheng
Jinan University; Zhuhai Trinomab Biotechnology Co., Ltd.
Hua-Xin Liao
Jinan University; Zhuhai Trinomab Biotechnology Co., Ltd.
Fei Xiao
Sun Yat-sen University
Hong Shan
Sun Yat-sen University
Shoudeng Chen (chenshd5@mail.sysu.edu.cn)
Sun Yat-sen University https://orcid.org/0000-0002-7634-2141

Article

Keywords: human monoclonal antibody, COVID-19, SARS-CoV-2, nucleocapsid protein, crystal structure, complement hyperactivation, viral protein targeting therapy, MASP-2

Posted Date: December 2nd, 2020

DOI: https://doi.org/10.21203/rs.3.rs-106760/v1

Version of Record: A version of this preprint was published at Nature Communications on May 11th, 2021. See the published version at https://doi.org/10.1038/s41467-021-23036-9.

A SARS-CoV-2 antibody curbs viral N protein-induced complement hyperactivation

Sisi Kang[1*], Mei Yang[1*], Suhua He[1*], Yueming Wang[2,3*], Xiaoxue Chen[1], Yao-Qing Chen[4], Zhongsi Hong[5], Jing Liu[6], Guanmin Jiang[7], Qiuyue Chen[1], Ziliang Zhou[1], Zhechong Zhou[1], Zhaoxia Huang[1], Xi Huang[8], Huanhuan He[1], Weihong Zheng[2,3], Hua-Xin Liao[2,3,#], Fei Xiao[1,5,#], Hong Shan[1,9,#], Shoudeng Chen[1,10,#]

1. Molecular Imaging Center, Guangdong Provincial Key Laboratory of Biomedical Imaging, The Fifth Affiliated Hospital, Sun Yat-sen University, Zhuhai, 519000, China
2. Institute of Biomedicine, Jinan University, Guangzhou, 510632, China
3. Zhuhai Trinomab Biotechnology Co., Ltd., Zhuhai, 519040, China
4. School of Public Health (Shenzhen), Sun Yat-sen University, Shenzhen, China
5. Department of Infectious Disease, The Fifth Affiliated Hospital, Sun Yat-sen University, Zhuhai, 519000, China
6. Department of Respiratory Disease, The Fifth Affiliated Hospital, Sun Yat-sen University, Zhuhai, 519000, China
7. Department of Clinical laboratory, The Fifth Affiliated Hospital of Sun Yat-sen University, Zhuhai, 519000, China
8. Center for Infection and Immunity, The Fifth Affiliated Hospital, Sun Yat-sen University, Zhuhai, 519000, China

9. Department of Intervention Medicine, The Fifth Affiliated Hospital, Sun Yat-sen University, Zhuhai, 519000, China
10. Department of Experimental Medicine, The Fifth Affiliated Hospital, Sun Yat-sen University, Zhuhai, 519000, China
* These authors contributed equally to this work
# Co-correspondence: Shoudeng Chen (chenshd5@mail.sysu.edu.cn); Hong Shan (shanhong@mail.sysu.edu.cn); Fei Xiao (xiaof35@mail.sysu.edu.cn); Hua-Xin Liao (tliao805@jnu.edu.cn)

Summary

Although human antibodies elicited by the severe acute respiratory syndrome coronavirus 2 (SARS-CoV-2) nucleocapsid (N) protein are profoundly boosted upon infection, little is known about the function of N-reactive antibodies. Herein, we isolated and profiled a panel of 32 N protein-specific monoclonal antibodies (mAbs) from a quick recovery coronavirus disease-19 (COVID-19) convalescent patient who had dominant antibody responses to the SARS-CoV-2 N protein rather than to the SARS-CoV-2 spike (S) protein. The complex structure of the N protein RNA binding domain with the mAb with the highest binding affinity (nCoV396) revealed changes in the epitopes and antigen's allosteric regulation. Functionally, a virus-free complement hyperactivation analysis demonstrated that nCoV396 specifically compromises the N protein-induced complement hyperactivation, which is a risk factor for the morbidity and mortality of COVID-19 patients, thus laying the foundation for the identification of functional anti-N protein mAbs.

Keywords: human monoclonal antibody, COVID-19, SARS-CoV-2, nucleocapsid protein, crystal structure, complement hyperactivation, viral protein targeting therapy, MASP-2

Main

The fatality rate of critical condition coronavirus disease 2019 (COVID-19) patients is exceptionally high (40% - 49%)[1,2]. Acute respiratory failure and generalized coagulopathy are significant aspects associated with morbidity and mortality[3-5]. A subset of severe COVID-19 patients has distinct clinical features compared to classic acute respiratory distress syndrome (ARDS), with delayed onset of respiratory distress[6] and relatively well-preserved lung mechanics despite the severity of hypoxemia[7]. It has been reported that complement-mediated thrombotic microvascular injury in the lung may contribute to atypical ARDS features of COVID-19, accompanied by extensive deposition of the alternative pathway (AP) and lectin pathway (LP) complement components[8]. Indeed, complement activation is found in multiple organs of severe COVID-19 patients in several other studies[9,10], as well as in patients with severe acute respiratory syndrome (SARS)[11,12]. A recent retrospective observational study of 11,116 patients revealed that complement disorder was associated with the morbidity and mortality of COVID-19[13].

The nucleocapsid (N) protein of severe acute respiratory syndrome coronavirus 2(SARS-CoV-2), the etiology agent of COVID-19, is one of the most abundant viral structural proteins with multiple functions inside the viral particles, the host cellular environment, and in *ex vivo* experiments[14-20]. Among these functions, a recent preprint study found that the SARS-CoV-2 N protein bound to MBL (mannan-binding lectin)-associated serine protease 2 (MASP-2) and resulted in

complement hyperactivation and aggravated inflammatory lung injury[19]. Consistently, the highly pathogenic SARS-CoV N protein was also found to bind with MAP19, an alternative product of MASP-2[21].

Although systemic activation of complement plays a pivotal role in protective immunity against pathogens, hyperactivation of complement may lead to collateral tissue injury. Thus, how to precisely regulate virus-induced dysfunctional complement activation in COVID-19 patients remains to be elucidated. The SARS-CoV-2 N protein is a highly immunopathogenic viral protein that elicits high titers of binding antibodies in humoral immune responses[22-24]. Several studies have reported the isolation of human monoclonal antibodies (mAbs) targeting the SARS-CoV-2 spike (S) protein, helping explain the possible developing therapeutic interventions for COVID-19[22,25-29]. However, little is known about the potential therapeutic applications of N protein-targeting mAbs in the convalescent B cell repertoire. Herein, we report a human mAb derived from the COVID-19 convalescent patient that specifically targets the SARS-CoV-2 N protein and functionally compromises complement hyperactivation *ex vivo*.

Isolation of N protein-reactive mAbs

To profile the antibody response to the SARS-CoV-2 N protein in patients during the early recovery phase, we collected blood samples from six convalescent patients seven to 25 days after the onset of the disease symptoms. All patients recovered from COVID-19 during the outbreak in Zhuhai, Guangdong Province,

China, with ages ranging from 23 to 66 years **(Extended Data Table 1)**. Our work and use of patients' samples is in accordance with the declaration of Helsinki, medical ethics standards and China's laws. Our study was approved by the Ethics Committee of The Fifth Affiliated Hospital, Sun Yat-sen University, and all patients signed informed consent forms. SARS-CoV-2 nasal swabs reverse transcription polymerase chain reaction (RT-PCR) tests were used to confirm that all 6 COVID-19 patients were negative for SARS-CoV-2 at the time of blood collection. Plasma samples and peripheral blood mononuclear cells (PBMCs) were isolated for serological analysis and antibody isolation. Serum antibody titers to SARS-CoV-2 S and N proteins were measured by enzyme-linked immunosorbent assay (ELISA) (**Figure 1a, 1b, and Extended Data Table 1**). Serologic analysis demonstrated that serum antibody titers to the N protein were substantially higher than those to the S protein in most of the patients. For example, ZD004 and ZD006 had only minimal levels of antibody response to the S protein, while they had much higher antibody titers to the N protein. Notably, the time from disease onset to complete recovery from clinical symptoms of COVID-19 patient ZD006 was only 9 days **(Extended Data Table 1)**.

To take advantage of patient ZD006, who was still in the early recovery phase with a high possibility of a high percentage of antigen-specific plasma cells, single plasma cells (**Figure 1c**) with the phenotype of $CD3^-/CD14^-/CD16^-/CD235a^-/CD19^+/CD20^{low\text{-}neg}/CD27^{hi}/CD38^{hi}$ as well as antigen-specific memory B cells with the phenotype of $CD19^+/CD27^+$ (**Figure 1d**) were sorted from PBMCs of patient ZD006 by fluorescence-activated cell sorting (FACS). To ensure an

unbiased assessment, the sorting of antigen-specific memory B cells was carried out with combined probes for both fluorophore-labeled S and N recombinant proteins. Variable regions of immunoglobulin (Ig) heavy and light chain gene segment (V_H and V_L, respectively) pairs from the sorted single cells were amplified by RT-PCR, sequenced, annotated and expressed as recombinant mAbs using the methods described previously[30]. Recombinant mAbs were screened against SARS-CoV-2 S and N proteins. In total, we identified 32 mAbs that reacted with the SARS-CoV-2 N protein, including 20 mAbs from plasma cells and 12 mAbs from memory B cells **(Extended Data Table 2)**. We found that IgG1 is the predominant isotype at 46.9%, followed by IgG3 (25.0%), IgA (18.8%), IgG2 (6.3%) and IgM (3.1) (**Figure 1e**). V_H gene family usage in SARS-CoV-2 N protein-reactive antibodies was 18.8% for V_H1, 62.5% for V_H3, 9.4% for V_H4, 6.2% for V_H5 and 3.1% for V_H7, respectively (**Figure 1f**), which was similar to the distribution of V_H families collected in the NCBI database. Nine of 32 SARS-CoV-2 N protein-reactive antibodies had no mutations from their germline V_H and V_H gene segments (**Figure 1f, Extended Data Table 2**). The average mutation frequency of the remaining mutated antibodies was 5.3% (+/-3.6%) in V_H and 3.5% (+/-2.7%) in V_L.

Consistent with the lower serum antibody titers to the SARS-CoV-2 S protein, we identified only eight SARS-CoV-2 S protein-reactive mAbs, including 5 antibodies from plasma cells and three antibodies from memory B cells. The V_H gene segment of the S protein-reactive antibodies had either no (6/8) or minimal (1/300) mutations (**Figure 1g**). There were no significant differences in

complementarity-determining region 3 (CDR3) length in amino acid residues between the N- (**Figure 1h**) and S-reactive antibodies (**Figure 1i**).

Approximately a quarter of antibodies directed to the N protein (**Figure 1f**) and almost all of antibodies to the S protein that had no or minimal mutations from their germlines (**Figure 1g**) had a primary antibody response similar to other typical primary viral infections. However, relatively high V_H mutation frequencies (mean of 5.7%) of the majority of antibodies to the N proteins were more similar to the mutation frequencies of antibodies from the secondary responses to the influenza vaccination reported previously[31]. Although patient ZD006 was hospitalized for only nine days after the onset of COVID-19 symptoms, the patient had high serum antibody titers, and the majority of the isolated N-reactive antibodies had a high mutation frequency, whereas the S-reactive antibodies had no or minimal mutations. These results reflect a much stronger antigen stimulation to the host driven by the SARS-CoV-2 N protein than by the S protein.

Binding characterizations of anti-N mAbs

To determine the antigenic targets by the N-reactive antibodies, we next analyzed the binding activities by ELISA with variant constructs of the N protein (full length N protein (N-FL): 1-400; N protein N-terminal domain (N-NTD): 41-174; and N protein C-terminal domain (N-CTD): 250-364) (**Figure 2a**). Among the 32 mAbs that bound to N-FL, 13 antibodies bound to N-NTD, and one antibody bound to N-CTD (**Figure 2b**). A total of nine antibodies, including one antibody (nCoV400) that bound to N-CTD, seven mAbs (nCoV396, nCoV416,

nCoV424, nCoV425, nCoV433, nCoV454, and nCoV457) that bound to N-NTD and one mAb (nCoV402) that bound only to N-FL but not to the other variant N proteins, were chosen as representative antibodies for further studies. Purified antibodies were confirmed to bind the N-FL protein by ELISA (**Figure 2c**). The affinity of these antibodies to the N-FL protein was measured by surface plasmon resonance (SPR) (**Figure 2d**). In an effort to further characterize the functional and structural relationships, three antibodies, nCoV396, nCOV416 and nCOV457, were selected for the production of recombinant fragment antigen-binding (Fab) antibodies based on their unique characteristics. The mAb nCoV396 has a V_H mutation frequency of 2.8% but a high binding affinity with a K_D of 1.02 nM (**Figure 2d**) to the N protein. The mAbs nCOV416 and nCOV457 have high V_H mutations at 11.1% and 8.7%, respectively and have a binding affinity to the N protein with K_D values of 7.26 nM and 12.6 nM, respectively (**Figure 2d, Extended Data Table 3**).

Complex structure of mAb with N-NTD

To investigate the molecular interaction mechanism of the mAb nCoV396 with the N protein, we next solved the complex structure of the SARS-CoV-2 N-NTD with the nCoV396 Fab nCoV396Fab at a 2.1 Å resolution by X-ray crystallography. The final structure was fitted with the visible electron density spanning residues 49-173 (SARS-CoV-2 N-NTD), 1-220 (nCoV396Fab, the heavy chain of the Fab), and 1-213 (nCoV396Fab, the light chain of Fab, except for the residues ranging from 136-141). The complete statistics for the data collection, phasing, and refinement are presented in **Extended Data Table 4**.

With the help of the high-resolution structure, we were able to designate all complementarity-determining regions (CDRs) in nCoV396Fab as the following: light chain CDR1, residues 23-32 (L-CDR1), light chain CDR2, residues 51-54 (L-CDR2), light chain CDR3, residues 94-100 (L-CDR3), heavy chain CDR1, residues 26-33 (H-CDR1), heavy chain CDR2, residues 51-57 (H-CDR2), and heavy chain CDR3, residues 99-108 (H-CDR3). Among them, we identified the interaction interface between N-NTD and L-CDR1, L-CDR3, H-CDR1, H-CDR2, and H-CDR3 of nCoV396Fab with an unambiguous electron density map (**Figure 3a, Extended Data Figure 1a**).

The interacting CDRs pinch the CT tail of the SARS-CoV-2 N-NTD (residues ranging from 159 to 172), with extensive binding contacts and a buried surface area of 1,079 $Å^2$ **(Extended Data Table 5).** Light chain L-CDR1 and L-CDR3 of nCoV396Fab interact with residues ranging from 159-163 of N-NTD via numerous hydrophilic and hydrophobic contacts (**Figure 3b, Extended Data Figure 1b**). Notably, the SARS-CoV-2 N-NTD residue Q163 is recognized by the L-CDR3 residue T95 via a hydrogen bond and simultaneously stacks with the L-CDR3 residue W96 and the L-CDR1 residue Y31 (**Figure 3c**). In addition, a network of interactions from the heavy chain H-CDR2 and H-CDR3 of nCoV396Fab to residues 165-172 of N-NTD suggests that the conserved residue K169 of SARS-CoV-2 N-NTD has a critical role in nCoV396 antibody binding. K169 is recognized via hydrogen bonds with the E99 δ-carboxyl group and the T100, D102, S105 main-chain carbonyl groups inside the H-CDR3 of nCoV396Fab (**Figure 3d**). In addition, SARS-CoV-2 N-NTD L167 also interacts

with I33, V50, N57, and A59 of H-CDR1 and H-CDR2 of nCoV396Fab through hydrophobic interactions (**Figure 3e**). Interestingly, all three residues (Q163, L167, and K169) of SARS-CoV-2 N-NTD are relatively conserved in the highly pathogenic betacoronavirus N protein **(Extended Data Figure 2a)**, which implies that nCoV396 may cross-interact with the SARS-CoV N protein or the Middle East respiratory syndrome coronavirus (MERS-CoV) N protein. Indeed, the binding affinities measured by SPR analysis demonstrate that nCoV396 interacts with the SARS-CoV N protein and the MERS-CoV N protein with a K_D of 7.4 nM **(Extended Data Figure 2b - c)**.

To discover the conformational changes between the SARS-CoV-2 N-NTD apo-state and the antibody-bound state, we next superimposed the complex structure with the N-NTD structure (PDB ID: 6M3M)[14]. The superimposition results suggest that the CT tail of SARS-CoV-2 N-NTD unfolds from the basic palm region upon nCoV396Fab binding (**Figure 3f**), which likely contributes to the allosteric regulation of the normal full-length N protein function. Additionally, nCoV396Fab binding results in a 7.4 Å movement of the β-finger region outward from the RNA binding pocket, which may enlarge the RNA binding pocket of the N protein (**Figure 3f**).

In summary, our crystal structural data demonstrated that the human mAb nCoV396 recognizes the SARS-CoV-2 N protein via a pinching model, resulting in a dramatic conformational change in residues 159 to 172, which is the linker region of N-NTD that is connected with other domains.

MAb curbs N-induced complement activation

Although a recent study suggests that the complement cascade is hyperactive by the N protein in the lungs of COVID-19 patients *via* the lectin pathway[19], it is unclear how to develop a virus-free and an effective system for analyzing the role of the SARS-CoV-2 N protein on complement hyperactivation. To this end, we developed a clinical autoimmune disease serum-based protease enzymatic approach to assess complement activation levels in the presence of the SARS-CoV-2 N protein. Since complement activation initiated by the lectin pathway features MASP-2 proteases by specific activity for cleaving complement components 2 and 4 (C2 and C4)[32], we designed a C2 internal quenched fluorescent peptide-based analysis route for *ex vivo* complement hyperactivation (**Figure 4a**). Briefly, serum was collected from the peripheral blood of volunteers with an autoimmune disease, as their serum contains the necessary components for complement activation characterized by elevated C3 levels **(Extended Data Table 6)**. Next, we collected the fluorescence signal from cleaved C2 synthetic peptide substrates (2Abz-SLGRKIQI-Lys(Dnp)-NH_2) in reaction mixtures containing autoimmune disease serum in the absence or presence of the SARS-CoV-2 N protein with or without the mAb nCoV396. The initial reaction rate (v_0) was estimated at a single concentration of individual sera from duplicate measurements over a range of substrate concentrations. The steady-state reaction constants maximal velocity (V_{max}) and Michaelis constant (K_m) were determined for comparisons (**Figure 4a**).

As shown in **Figure 4b**, the calculated V_{max} of reactions without any other exogenous proteins is 1.49 response units (RU)·s^{-1}. Additions of the SARS-CoV-2 N protein (concentrations ranging from 0.5 μM to 10 μM) in the reactions remarkably elevate the V_{max} up to 2-fold, ranging from 2.37 ~ 3.02 RU·s^{-1}. Similarly, additions of the SARS-CoV-2 N protein led to an approximate 1.8-fold increase in the V_{max}/K_m values, which suggested that the specificity constant (K_{cat}/K_m) of MASP-2 to substrates is increased in the presence of the viral N protein as the enzyme concentrations are equivalent among the reactions **(Extended Data Table 7 - 8)**. To confirm the kinetic analyses, Hanes plots ([S]/V versus [S]) were also drawn and found to be linear (**Figure 4c**). Therefore, the addition of the SARS-CoV-2 N protein does not change the single substrate binding site characterization of the enzymatic reactions. To assess the suppression ability of nCoV396 to the SARS-CoV-2 N protein-induced complement hyperactivation function, we next conducted complement hyperactivation analyses at various N protein: nCoV396 ratios. As shown in **Figure 4d**, the addition of the N protein elevates the V_{max} value up to 40-fold (1:0 ratio), whereas the addition of the antibody nCoV396 decreases the V_{max} in a dose-dependent manner **(Extended Data Table 9)**. To further validate the function of nCoV396, we next performed complement hyperactivation analyses in five other serum samples from autoimmune disease donors. Consistently, the V_{max} of reactions was boosted in the presence of the N protein in all samples but declined in the presence of both the mAb nCoV396 and the N protein (**Figure 4e)**. In conclusion, these results demonstrate that the SARS-CoV-2 N protein is

capable of inducing complement hyperactivation *ex vivo*, not only by facilitating the V_{max} of MASP-2 catalytic activity but also by enhancing the substrate binding specificity in the reactions. The N-reactive mAb nCoV396 specifically compromises the SARS-CoV-2 N protein-induced complement hyperactivation within clinical serum samples.

Discussion

From a quickly recovered COVID-19 patient, we isolated 32 mAbs specifically targeting the SARS-CoV-2 N protein. The binding affinity of mAbs ranged from 1 nM to 25 nM, which is comparable with the binding affinity of mature S protein-reactive antibodies[22,25-29] and the other mature antibodies identified during acute infections[33,34]. The characteristics of the isolated N-reactive mAbs are different from those of the isolated S-reactive mAbs in COVID-19 patients during the early recovery phase, suggesting that sampling time is pivotal for identifying differential immune responses to different SARS-CoV-2 viral proteins.

The crystal structure of nCoV396 bound to SARS-CoV-2 N-NTD elucidates the interaction mechanism of the complex between the first reported N protein-reactive human mAb and its targeted N protein. Three conserved amino acids (Q163, L167, and K169) in the N protein are responsible for nCoV396 recognition, which provides evidence of cross-reactivity of nCoV396 to the N protein of SARS-CoV or MERS-CoV. Intriguingly, the nCoV396 binding of SARS-CoV-2 N-NTD undergoes several conformational changes, resulting in an enlargement of the N-NTD RNA binding pocket enlargement and partial unfolding of the basic

palm region. More importantly, this conformational change occurs in the CT tail of the N-NTD, which may alter the positioning of individual domains in the context of the full-length protein and lead to a potential allosteric effect for protein functions.

Complement is one of the first lines of defense in innate immunity and is essential for cellular integrity and tissue homeostasis and for modifying the adaptive immune response[35]. Emerging evidence suggests that the complement system plays a vital role in a subset of critical COVID-19 patients, with features of atypical acute respiratory distress syndrome, disseminated intravascular coagulation, and multiple organ failure[9,10,36]. A few pieces of evidence show that the N protein of highly pathogenic coronaviruses (SARS-CoV-2 and SARS-CoV) is involved in the initiation of MASP-2-dependent complement activation[19,21]. Encouragingly, critical COVID-19 patients treated with complement inhibitors, including small molecules to the complement component C3 and an antibody targeting the complement component C5, show remarkable therapeutic outcomes[19]. Currently, there are 11 clinical trials related to targeting the complement pathway (https://clinicaltrials.gov). To avoid adverse effects of human complement component-targeting therapy, a viral protein-specific approach is warranted. The antibody nCoV396 isolated from COVID-19 convalescent patients is an excellent potential candidate with a high binding affinity to the N protein and high potency to inhibit complement hyperactivation. As revealed by atomic structural information, the binding may allosterically change the full-length N protein conformation. To determine the role of nCoV396 in the suppression of complement hyperactivation, we monitored MASP-2

protease activity based on its specific fluorescence-quenched C2 substrate in sera from autoimmune disease patients. The complete complement components in the sera of patients with autoimmune disorders allow us to monitor the activating effects of the SARS-CoV-2 N protein and its specific mAbs. Although we cannot calculate the other steady-state enzymatic reaction constants as the precise concentration of MASP-2 in serum is unknown, we identified the V_{max} of the specific C2 substrate for the enzymatic reaction. We demonstrated that the SARS-CoV-2 N protein elevated the V_{max} of the reaction, up to 40-fold, in the sera of all 7 individuals tested, while nCoV396 effectively suppressed the V_{max} of the reaction mixtures. These results indicated that serum-based complement activation analysis of autoimmune disease patients is a virus-free and an effective method for examining complement activation mediated by the SARS-CoV-2 N protein.

Although the precise interaction of the SARS-CoV-2 N protein with MASP-2 remains to be elucidated, our work defined the region on the SARS-CoV-2 N protein recognized by the mAb nCoV396 that plays an important role in complement hyperactivation and indicates that human mAbs from convalescents could be a promising potential therapeutic candidate for the treatment of COVID-19.

References

1 Epidemiology Working Group for Ncip Epidemic Response, Chinese Center for Disease Control and Prevention. [The epidemiological

characteristics of an outbreak of 2019 novel coronavirus diseases (COVID-19) in China]. *Zhonghua Liu Xing Bing Xue Za Zhi* **41**, 145-151 (2020)

2 Wiersinga, W. J., Rhodes, A., Cheng, A. C., Peacock, S. J. & Prescott, H. C. Pathophysiology, Transmission, Diagnosis, and Treatment of Coronavirus Disease 2019 (COVID-19): A Review. *Jama-J. Am. Med.* Assoc. doi:10.1001/jama.2020.12839 (2020).

3 Tang, N., Li, D. J., Wang, X. & Sun, Z. Y. Abnormal coagulation parameters are associated with poor prognosis in patients with novel coronavirus pneumonia. *J Thromb. Haemost.* **18**, 844-847 (2020).

4 Wang, D. W. *et al.* Clinical Characteristics of 138 Hospitalized Patients With 2019 Novel Coronavirus-Infected Pneumonia in Wuhan, China. *Jama-J. Am. Med. Assoc.* **323**, 1061-1069 (2020).

5 Zhu, N. *et al.* A Novel Coronavirus from Patients with Pneumonia in China, 2019. *N. Engl. J. Med.* **382**, 727-733 (2020).

6 Zhou, F. *et al.* Clinical course and risk factors for mortality of adult inpatients with COVID-19 in Wuhan, China: a retrospective cohort study. *Lancet* **395**, 1054-1062 (2020).

7 Gattinoni, L. *et al.* COVID-19 Does Not Lead to a "Typical" Acute Respiratory Distress Syndrome. *Am. J. Respir. Crit. Care Med* **201**, 1299-1300, (2020).

8 Magro, C. *et al.* Complement associated microvascular injury and thrombosis in the pathogenesis of severe COVID-19 infection: A report of five cases. *Transl. Res.* **220**, 1-13 (2020).

9 Cugno, M. *et al.* Complement activation in patients with COVID-19: A novel therapeutic target. *J. Allergy Clin Immunol* **146**, 215-217, (2020).

10 Noris, M., Benigni, A. & Remuzzi, G. The case of complement activation in COVID-19 multiorgan impact. *Kidney Int*. **98**, 314-322 (2020).

11 Pang, R. T. *et al.* Serum proteomic fingerprints of adult patients with severe acute respiratory syndrome. *Clin. Chem.* **52**, 421-429, (2006).

12 Chen, J. H. *et al.* Plasma proteome of severe acute respiratory syndrome analyzed by two-dimensional gel electrophoresis and mass spectrometry. *Proc. Natl. Acad. Sci. U. S. A.* **101**, 17039-17044 (2004).

13 Ramlall, V. *et al.* Immune complement and coagulation dysfunction in adverse outcomes of SARS-CoV-2 infection. *Nat. Med.* (2020).

14 Kang, S. *et al.* Crystal structure of SARS-CoV-2 nucleocapsid protein RNA binding domain reveals potential unique drug targeting sites. *Acta Pharm. Sin. B*, doi:10.1016/j.apsb.2020.04.009 (2020).

15 Ye, Q., West, A. M. V., Silletti, S. & Corbett, K. D. Architecture and self-assembly of the SARS-CoV-2 nucleocapsid protein. *Protein Sci.*, doi:10.1002/pro.3909 (2020).

16 Iserman, C. *et al.* Specific viral RNA drives the SARS CoV-2 nucleocapsid to phase separate. *bioRxiv*, doi:10.1101/2020.06.11.147199 (2020).

17 Li, J. Y. *et al.* The ORF6, ORF8 and nucleocapsid proteins of SARS-CoV-2 inhibit type I interferon signaling pathway. *Virus Res.* **286**, 198074, (2020).

18 Perdikari, T. M. *et al.* SARS-CoV-2 nucleocapsid protein undergoes liquid-liquid phase separation stimulated by RNA and partitions into phases of human ribonucleoproteins. *bioRxiv*, doi:10.1101/2020.06.09.141101 (2020).

19 Gao, T. *et al.* Highly pathogenic coronavirus N protein aggravates lung injury by MASP-2-mediated complement over-activation. *medRxiv*, 2020.2003.2029.20041962, doi:10.1101/2020.03.29.20041962 (2020).

20 Guo, Y. R. *et al.* The origin, transmission and clinical therapies on coronavirus disease 2019 (COVID-19) outbreak - an update on the status. *Military Med. Res.* **7**, 11 (2020).

21 Liu, J. L., Cao, C. & Ma, Q. J. Study on interaction between SARS-CoV N and MAP19. *Xi bao yu fen zi mian yi xue za zhi = Chinese journal of cellular and molecular immunology* **25**, 777-779 (2009).

22 Chi, X. *et al.* A neutralizing human antibody binds to the N-terminal domain of the Spike protein of SARS-CoV-2. *Science 369*, 650-655 (2020).

23 Klasse, P. J. & Moore, J. P. Antibodies to SARS-CoV-2 and their potential for therapeutic passive immunization. *Elife* **9**, e57877 (2020).

24 Kreer, C. *et al.* Longitudinal Isolation of Potent Near-Germline SARS-CoV-2-Neutralizing Antibodies from COVID-19 Patients. *Cell* S0092-8674**(20*)**, 30821-30827 (2020).

25 Zost, S. J. *et al.* Potently neutralizing and protective human antibodies against SARS-CoV-2. *Nature*, doi:10.1038/s41586-020-2548-6 (2020).

26 Wu, Y. *et al.* A noncompeting pair of human neutralizing antibodies block COVID-19 virus binding to its receptor ACE2. *Science* **368**, 1274-1278, (2020).

27 Wang, C. *et al.* A human monoclonal antibody blocking SARS-CoV-2 infection. *Nat. Commun.* **11**, 2251 (2020).

28 Ju, B. *et al.* Human neutralizing antibodies elicited by SARS-CoV-2 infection. *Nature* **584**,115-119 (2020).

29 Cao, Y. *et al.* Potent Neutralizing Antibodies against SARS-CoV-2 Identified by High-Throughput Single-Cell Sequencing of Convalescent Patients' B Cells. *Cell* **182**, 73-84 (2020).

30 Liao, H. X. *et al.* High-throughput isolation of immunoglobulin genes from single human B cells and expression as monoclonal antibodies. *J. Virol. Methods* **158**, 171-179 (2009).

31 Moody, M. A. *et al.* H3N2 influenza infection elicits more cross-reactive and less clonally expanded anti-hemagglutinin antibodies than influenza vaccination. *PLoS One* **6** (10): e25797 (2011).

32 Duncan, R. C. *et al.* Multiple domains of MASP-2, an initiating complement protease, are required for interaction with its substrate C4. *Mol. Immunol.* **49**, 593-600 (2012).

33 Stettler, K. *et al.* Specificity, cross-reactivity, and function of antibodies elicited by Zika virus infection. *Science* **353**, 823-826 (2016).

34 Yu, L. *et al.* Delineating antibody recognition against Zika virus during natural infection. *JCI Insight* **2** (12):e93042 (2017).

35 Zipfel, P. F. & Skerka, C. Complement regulators and inhibitory proteins. *Nat. Rev. Immunol.* **9**, 729-740 (2009).

36 Lo, M. W., Kemper, C. & Woodruff, T. M. COVID-19: Complement, Coagulation, and Collateral Damage. *J. Immunol*, doi: 10.4049/jimmunol.2000644 (2020).

Methods

Recombinant SARS-CoV-2 S-ECD and N proteins.

Recombinant SARS-CoV-2 S protein (extracellular domain of the S protein (ECD) with His and FLAG Tags, Z03481) was purchased from GenScript. SARS-CoV-2 (formerly known as 2019-nCoV, recombinant full-length N protein with a CT 6x His tag (His tag, 40588-V08B) was purchased from Sino Biological. The SARS-CoV-2 N protein expression plasmid (SARS-CoV N-FL) was a gift from the Guangdong Medical Laboratory Animal Center. SARS-CoV and MERS-CoV N-FL were purchased from RuiBiotech. SARS-CoV-2 N-FL (residues 1 to 419), SARS-CoV-2 N-NTD domain (residues 41 to 174), SARS-CoV-2 N-CTD domain (residues 250 to 364), SARS-CoV N-FL and MERS-CoV N-FL were cloned into the pET-28a vector and expressed in the Rosetta *E. coli* strain. Expression of SARS-CoV-2 N-FL and variants in *E. coli* was induced with 0.1 mM isopropylthio-β-galactoside (IPTG) and cultured overnight at 16 °C in Terrific Broth media. Expressed recombinant N proteins were initially purified by using nickel column chromatography and further purified via size-exclusion chromatography.

PBMCs from COVID-19 patients and sorting of single plasma cells and memory B cells by FACS

Blood samples were collected 9 - 25 days after the onset of the disease from patients who had recovered from COVID-19 infection. PBMCs and plasma were isolated from blood samples by Ficoll-Paque PLUS (GE, 17-1440-02) density gradient centrifugation. All work related to human subjects was carried out in

compliance with Institutional Review Board protocols approved by the Institutional Review Board of the Fifth Affiliated Hospital of Sun Yat-sen University. Single plasma cells with the surface markers $CD3^-$, $CD14^-$, $CD16^-$, $CD235a^-$, $CD19^+$, $CD20^{low\text{-}neg}$, $CD27^{hi}$ and $CD38^{hi}$ and memory B cells with the surface markers $CD3^-$, $CD14^-$, $CD16^-$, $CD235a^-$, $CD20^-$, $CD19^+$, $CD27^+$, SARS-CoV-2 S^+ and SARS-CoV-2 N^+ (BD Biosciences and Invitrogen) were sorted into individual wells in 96-well microtiter plates containing cell lysis and RT buffer for Ig gene amplification by fluorescence activated cell sorting (FACS) as previously described[37] on a BD FACS Aria SORP. Data were analyzed using BD FACS Diva 8.0.1 software.

Isolation and expression of Ig V_H and V_L genes

Genes encoding V_H and V_L were amplified by reverse transcription (RT) and nested primer chain reaction (PCR) and nested PCR using the method previously described[38]. PCR products of Ig V_H and V_L genes were purified using a PCR purification kit (QIAGEN), sequenced in forward and reverse directions (Thermo Fisher scientific) and annotated by using IMGT/V-QUEST (www.imgt.org/IMGT_vquest). Functional V_H and V_L genes were used for assembling full-length Ig heavy and light chain linear expression cassettes by one-step overlapping PCR[38]. HEK-293T cells in 12-well plates were transfected with the assembled Ig heavy and light chain pairs derived from the same single individual plasma cells using Effectene (QIAGEN) as the transfection reagent[38].

Production of recombinant IgG and Fab antibodies

For the production of purified full-length IgG1 antibodies, the V_H and V_L genes were cloned into the pCDNA3.1$^+$ (Invitrogen)mammalian expression vector containing either the human IgG1 constant region gene, the human kappa light chain constant region gene or the lambda light chain constant region gene using standard recombinant DNA technology[38]. For the production of the purified nCoV396Fab antibody, a stop codon TGA was introduced after the sequence (5′-TCTTGTGACAAA-3′), which encodes the amino acid residues SCDK, just before the hinge of the human IgG1 constant region[39]. Recombinant IgG1 antibodies and the nCoV396Fab antibody were produced in 293F cells cultured in serum-free medium by cotransfection with the generated IgG1 full-length or Fab heavy- and light chain gene expression plasmid pairs using polyethylenimine[40]. Full-length IgG1 antibodies were purified by using Protein A column chromatography as described previously[38]. The nCoV396Fab antibody used for the crystal structure was purified by Lambda FabSelect, an affinity resin designed for the purification of human Fab with a lambda light chain (GE Healthcare)[39].

Analysis of the binding of plasma antibodies and isolated mAbs to the S and N proteins by ELISA

We collected plasma from 6 patients and measured serum antibody titers using recombinant SARS-CoV-2 S and N proteins as antigens to coat ELISA plates. Antibodies in the supernatant of the transfected 293T cultures harvested 3 days after transfection were screened by ELISA as described previously[38]. The binding of purified antibodies to the N or S protein was also analyzed by ELISA. Briefly, all protein antigens (S, N-FL, N-NTD (41-174), and N-CTD (250-364)) were used

505 at 200 ng/well to coat 96-well high-binding ELISA plates (Nunc 442404) using
506 carbonate-bicarbonate buffer at pH 9.6. Plates were incubated overnight at 4 °C
507 and blocked at room temperature for 2 h with PBS blocking buffer containing 5%
508 w/v goat serum and 0.05% Tween-20. Plasma or supernatant of transfected
509 293T cell cultures or purified mAbs in serial dilutions in PBS were incubated at
510 37 °C for 1 h. Goat anti-human IgG-horseradish peroxidase (HRP, 1:10,000
511 dilution) (Promega, W4031) as the secondary antibody diluted in blocking buffer
512 was added and incubated at 37 °C for 1 h. These plates were then washed 5
513 times with PBS and developed with 100 μL of 3,3',5,5'-Tetramethylbenzidine
514 (TMB) substrate/well (Solarbio PR1200). The reaction of the plates was stopped
515 with 50 μL of 2 M H_2SO_4/well and read at a wavelength of 450 nm by an ELISA
516 reader. The relative affinity of mAbs to the N protein antigen was determined as
517 the effective concentration (EC_{50}) of the antibody resulting in half maximal
518 binding to the antigen by curve fitting with GraphPad Prism software.

519 **Affinity and kinetic measurements by SPR**

520 The binding affinity (K_D), association rate (k_a) and dissociation rate (k_d) of purified
521 mAbs to the N protein were determined by SPR using a Biacore X100 System.
522 Anti-human Fc IgG antibody was first immobilized on a CM5-chip to
523 approximately 6,000 RU by covalent amine coupling using a human antibody
524 capture kit (GE Healthcare). Purified mAbs were captured on channel 2 of the
525 CM5 chip to approximately 200 RU. Five 2-fold serial dilutions of the N protein
526 starting at 40 μg/ml, 20 μg/ml, 10 μg/ml or 4 μg/ml were injected at a rate of 30
527 μL/min for 90 s with a 600 s dissociation. The chip was regenerated by injection

of 3 M $MgCl_2$ for 30 s. All experiments were performed at room temperature, and data were analyzed using Biacore X100 Evaluation Software (version: 2.0.1). Curves were fitted to a 1:1 binding model to determine the kinetic rate constants (k_a and k_d). K_D values were calculated from these rate constants.

Crystallization and data collection

SARS-CoV-2 N-NTD (41–174) was cloned into the pRSF-Duet-1 vector with an NT 6x His-SUMO tag, recombinantly expressed in *E. coli* and purified as an NT 6x His-Sumo-tagged protein. After Ni column chromatography followed by ulp1 digestion for tag removal, the SARS-CoV-2 N-NTD (41–174) protein was further purified via size-exclusion chromatography. Prior to crystallization, the SARS-CoV-2 N-NTD (41–174) sample was mixed with nCoV396Fab at a 1:1.5 molar ratio for approximately half an hour and then further purified via size-exclusion chromatography. Crystals were grown by the sitting drop method using a Mosquito LCP crystallization robot with 0.3 μL of protein (6 mg/ml) mixed with 0.3 μL of well solution at 16 °C. Better crystals were obtained in 0.01 M calcium chloride dihydrate, 0.05 M sodium cacodylate trihydrate (pH 7.2), 1.675 M ammonium sulfate and 0.5 mM spermine. The crystals were harvested after 3 days. Crystals were frozen in liquid nitrogen in the reservoir solution supplemented with 25% glycerol (v/v) as a cryoprotectant. X-ray diffraction data were collected at the Shanghai Synchrotron Radiation Facility BL18U at a wavelength of 0.979 Å and a temperature of 100 K. The complex structure of SARS-CoV-2 N-NTD with the mAb nCoV396 was determined by Phenix molecular replacement using the SARS-CoV-2 N-NTD structure (PDB ID: 6M3M)

and the monoclonal antibody omalizumab Fab (PDB ID: 6TCN) as the search models. The X-ray diffraction and structure refinement statistics are summarized in Extended Data Table 4. The final Ramachandran statistics are 97.1% favored, 2.9% allowed and 0.0% outliers.

Fluorescence-quenched substrate assays

The fluorescence-quenched substrate (FQS) [C2 P4–P4′ (2Abz-SLGRKIQI-Lys(Dnp)-NH2)] was synthesized and purified in greater than 90% purity by Sangon Biotech (Shanghai, China). The FQS was solubilized in 50% (v/v) dimethylformamide (DMF). Assays were carried out in fluorescence assay buffer (FAB) (0.05 M Tris–HCl, 0.15 M NaCl, 0.2% (w/v) PEG 8,000, and pH 7.4) at 37 °C using final substrate concentrations in the range of 2.8125–90 μM. A range of substrate dilutions, performed in triplicate, were prepared in FAB and were added to the wells at 100 μl/well in the assay plates. The plates were incubated at 37 °C for 10 minutes. Five microliters of serum from autoimmune patients was added to the mixture of the SARS-CoV-2 N protein with nCoV396 at a 1:1.2 molar ratio in the assay plates. Fluorescence intensity was measured on an EnVision 2015 Multimode plate reader (PerkinElmer) at an excitation wavelength of 320 nm and an emission wavelength of 420 nm for the FQS. The initial reaction rate was estimated at a single concentration of enzyme from duplicate measurements over a range of substrate concentrations. To determine steady-state reaction constants (V_{max}, half saturation constant ($K_{0.5}$) and Hill coefficient(h)), the experimental results were fitted using GraphPad Prism Version 8.0 (GraphPad Software, San Diego, CA) to an equation describing

positive cooperativity: $Y = V_{max} \times \frac{X^h}{K0.5^h + X^h}$, where 0.5 defines the relationship between the reaction rate (V) and the substrate concentration ([S]) when more than one binding site applies.

Methods references

37. Morris, L. et al. Isolation of a human anti-HIV gp41 membrane proximal region neutralizing antibody by antigen-specific single B cell sorting. *PloS one* **6**, e23532 (2011).

38. Liao, H. X. et al. High-throughput isolation of immunoglobulin genes from single human B cells and expression as monoclonal antibodies. *J. Virol. Methods* **158**, 171-179 (2009).

39. Nicely, N. I. et al. Crystal structure of a non-neutralizing antibody to the HIV-1 gp41 membrane-proximal external region. *Nat. Struct. Mol. Biol.* **17**, 1492-1494 (2010).

40. Smith, K. et al. Rapid generation of fully human monoclonal antibodies specific to a vaccinating antigen. *Nat. Protoc.* **4**, 372-384 (2009).

Acknowledgement

This work is supported by the COVID-19 Emerging Prevention Products, Research Special Fund of Zhuhai City (ZH22036302200016PWC to S.C.; ZH22036302200028PWC to F. X.; ZH22046301200011PWC to H-X. L.); Emergency Fund from Key Realm R&D Program of Guangdong Province (2020B111113001) to H.S.; Zhuhai Innovative and Entrepreneurial Research Team Program (ZH01110405160015PWC, ZH01110405180040PWC) to H-X. L; We thank the staffs of the BL18U/19U/17U beamlines at SSRF for their help with the X-ray diffraction data screening and collections. We thank Junlang Liang, Tong Liu, Nan Li, Xiaoli Wang, Zhenxing Jia, and Jiaqi Li from Zhuhai Trinomab Biotechnology Co., Ltd. for technical assistants of mAbs isolation, production and characterization.

Author Contributions

S. C., H. S., F. X. and H-X. L. contributed the conception of the study and established the construction of the article. S. C. and H-X. L. designed the experiments and wrote the manuscript. S. K., M. Y., S. H. contributed to protein purification and crystallization, *in vitro* protein-protein interaction analysis, and complement activation analysis. Y. W. contributed to mAbs isolation, *in vitro* protein-protein interaction analysis. S. C., S. K. M. Y., and S. H. performed structural determination and validation. S. C., S. K., Y. W. drew figures. X. C., Y. C., Q. C., Z. Z., Z. Z., Z. H., X. H., H. S., W. Z., and H. H. contributed to

610 interpretation of data. Z. H., J. L., G. J., and F. X. contributed to clinical samples
611 collections. S.K., M.Y., S. H., Y.W. contributed equally to this work.

612 Conflict of Interest

613 The authors declare no conflict of interest.

614 Data availability statement

615 The structure in this paper is deposited to the Protein Data Bank with 7CR5
616 access code.

617 Additional Information

618 Correspondence and requests for materials should be addressed to Shoudeng
619 Chen (chenshd5@mail.sysu.edu.cn) and/or Hua-Xin Liao (tliao805@jnu.edu.cn).

Figures

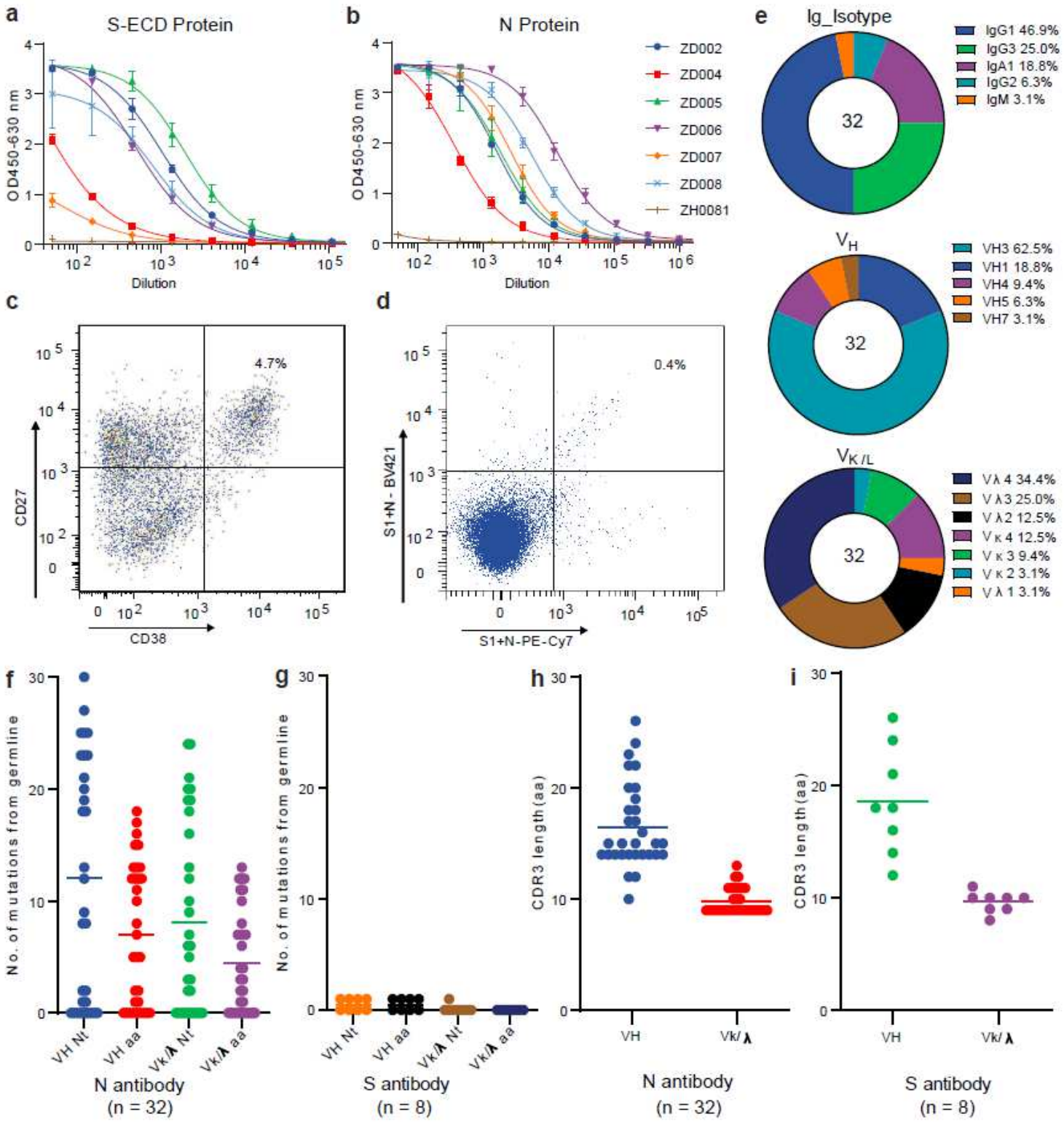

Figure 1

Acquisition and characterization of antibodies. Serum antibody titers of six SARS-CoV-2 convalescent patients to the SARS-CoV-2 S (a) and N (b) proteins measured by ELISA. Sorting of single plasma cells (c) with CD38 and CD27 double-positive B cells and single N and S proteinspecific memory B cells (d) by

FACS. (e) Percentage of different isotypes, VH and VL gene families of 32 isolated N-reactive antibodies. (f) Number of mutations in nucleotides and amino acids in VH and VL (Vκ and Vλ) of 32 N-reactive antibodies and eight S-reactive antibodies (g). Length of the 32 Nreactive antibodies (h) and eight S-reactive antibodies (i) in H-CDR3.

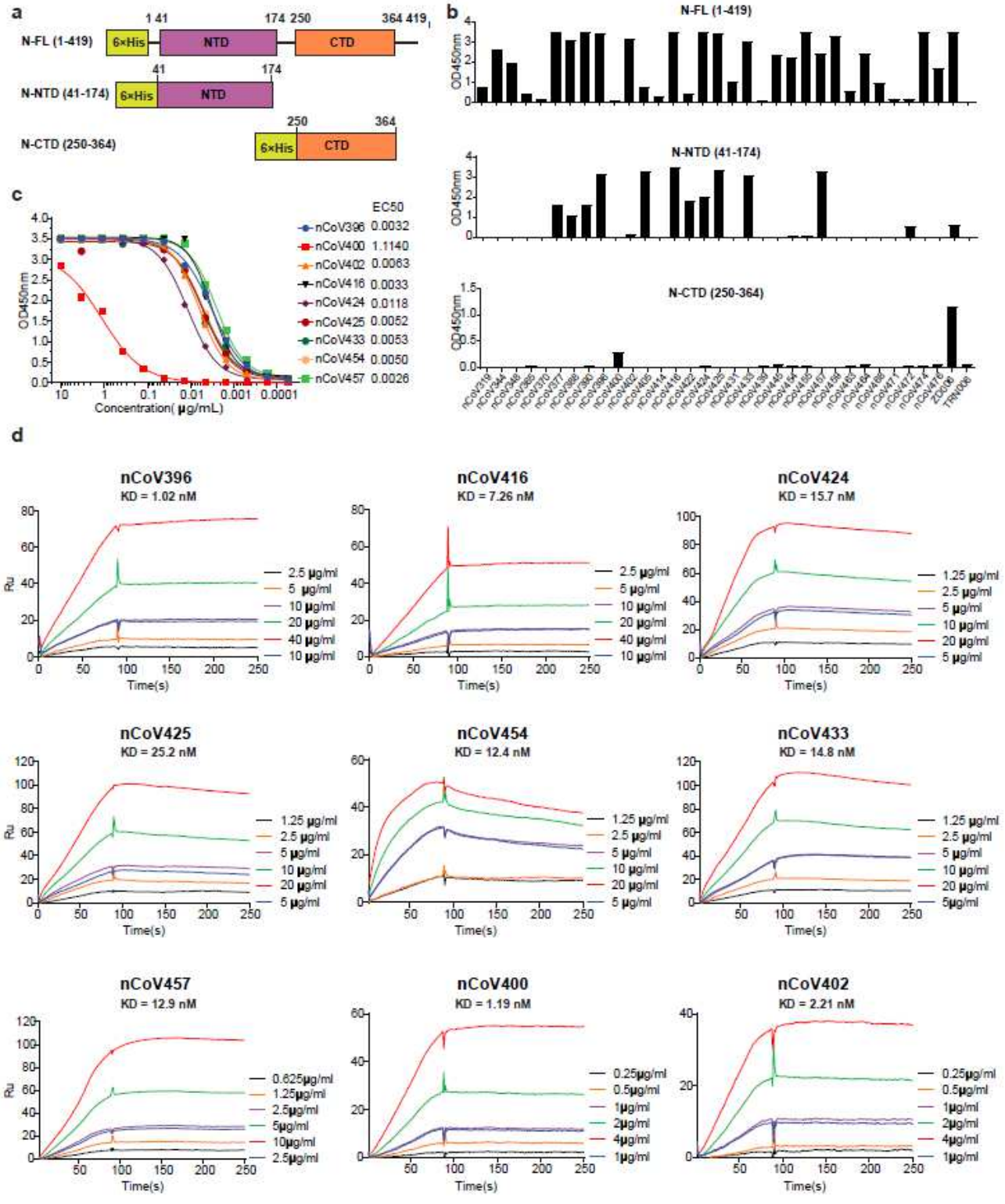

Figure 2

Reactivity and affinity of the isolated antibodies to the N protein antigens. (a) Schematic presentation of the SARS-CoV-2 N protein and two variants. (b) Antibodies expressed in transfected 293 cells were evaluated for binding to N-FL, N-NTD and N-CTD by ELISA. Plasma from patient ZD006 and an irrelevant mAb TRN006 were used as the positive control and negative control, respectively. (c) The ability of nine purified antibodies to the N-FL protein was determined by ELISA. (d) Binding affinity of nine selected antibodies to the N protein was measured by SPR. KD values are shown above the individual plots.

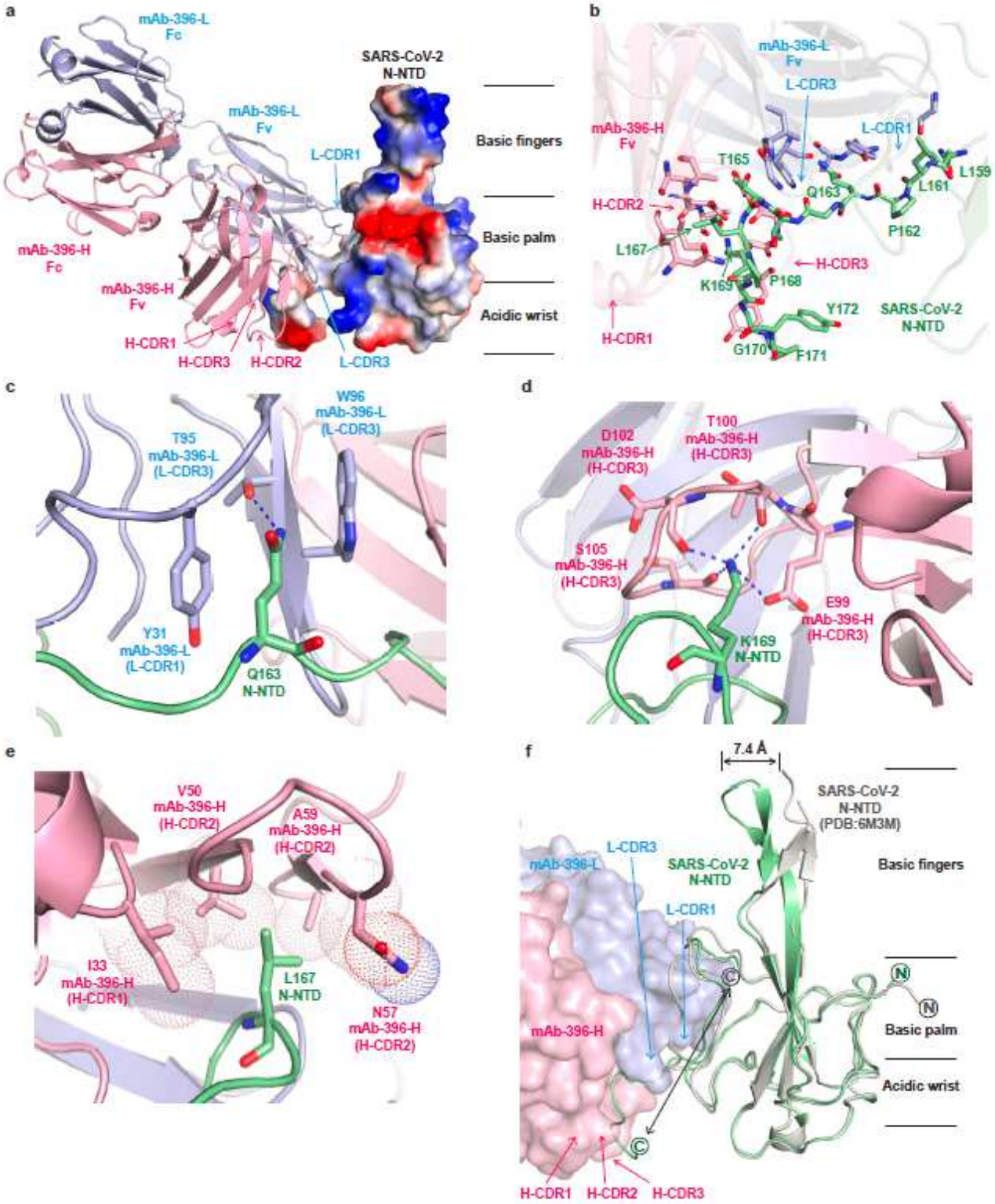

Figure 3

Complex structure of mAb nCoV396 with SARS-CoV-2 N-NTD(a) Overall structure of the mAb SARS-CoV-2 N-NTD complex. The light chain (pink) and heavy chain (blue) of mAb nCoV396 are illustrated with the ribbon representation. SARS-CoV-2 N-NTD is illustrated with an electrostatic surface, in which blue denotes a positive charge potential, while red indicates a negative charge potential. (b) The N-N□D epitope recognized by mAb nCoV396. The interacting residues of N-NTD and nCoV396 are highlighted with the stict representation. Recognition of Q163 (c),K169 (d) and L167 (e) in N-NTD by mAb nCoV396. The dashed blue line represents hydrogen bonds. Hydrophobic interactions are illustrated with the dot representation. (f) Conformational changes in N-NTD upon mAb nCoV396 binding. The apo structure of N-NTD is colored gray. Antibody-bound N-N□D is colored green. The N-terminus and C-terminus of the N-NTD are labeled with circles. mAb nCoV396 is illustrated with surface representation. All figures were prepared by PyMol.

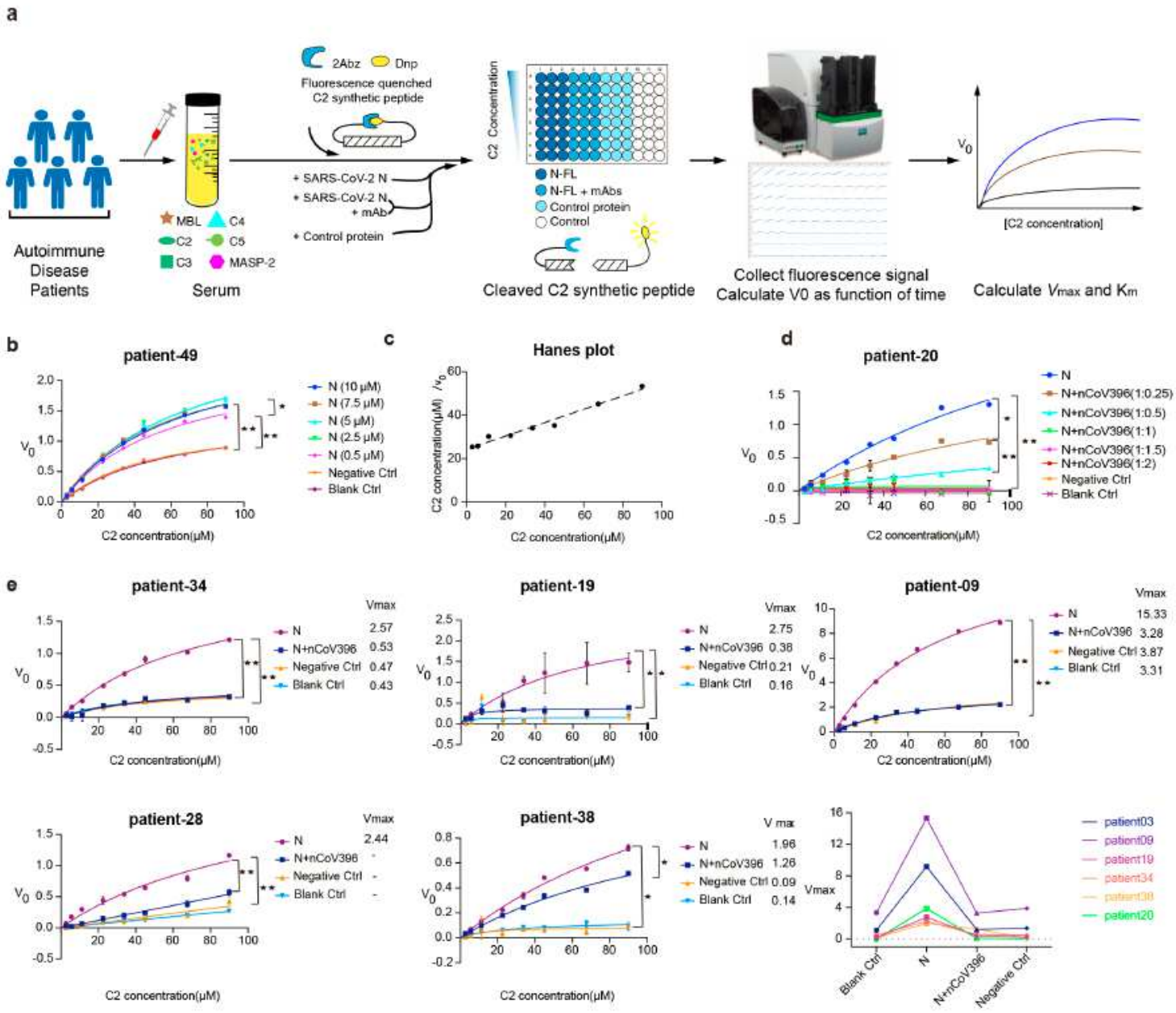

Figure 4

Antibody nCoV396 compromises SARS-CoV-2 N protein-induced complement hyperactivation. (a) Flow scheme of the SARS-CoV-2 N protein and nCoV396 influencing the protease activity of MASP-2 in the serum of autoimmune disease patients. The Michaelis-Menten curve shows the effect of increasing the N protein concentration (b) and antibody concentration (d) on the substrate C2 cleavage of MAPS-2 in the serum of patient 49 and patient 20. (c) A Hanes plot where C2 concentrationN0 is plotted against C2 concentration with the addition of 5 μM N protein. (e) The mAb nCoV396 inhibits the N protein-induced excessive cleavage of C2 in the serum of six autoimmune disease patients, and the last panel shows a summary of Vmax for all patients. Negative control (Negative Ctrl) and blank control (Blank Ctrl) represent reactions containing bovine serum albumin (BSA) instead of N or N+mAb and without exogenous protein, respectively. The mean and standard deviation (SD) values of three technical replicates are shown. P values: *P < 0.05; **P < 0.01; "-" indicates that the experimental kinetics did not conform to Michaelis-Menten kinetics.

Supplementary Files

This is a list of supplementary files associated with this preprint. Click to download.

- 5ExTFigTablesNC.pdf
- 4PDBNC.pdf